


Simultaneous imaging of the ferromagnetic and ferroelectric structure in multiferroic heterostructures

Journal Article

Author(s):

Unguris, John; Bowden, Samuel R.; Pierce, Daniel T.; [Trassin, Morgan](#) ; Ramesh, Rammamoorthy; Cheong, Sang-Wook; Fackler, Sean; Takeuchi, Ichiro

Publication date:

2014-07-18

Permanent link:

<https://doi.org/10.3929/ethz-b-000086915>

Rights / license:

[Creative Commons Attribution 3.0 Unported](#)

Originally published in:

APL Materials 2(7), <https://doi.org/10.1063/1.4890055>

Simultaneous imaging of the ferromagnetic and ferroelectric structure in multiferroic heterostructures

Cite as: APL Mater. 2, 076109 (2014); <https://doi.org/10.1063/1.4890055>

Submitted: 12 June 2014 . Accepted: 02 July 2014 . Published Online: 18 July 2014

J. Unguris, S. R. Bowden, D. T. Pierce, M. Trassin, R. Ramesh, S.-W. Cheong, S. Fackler, and I. Takeuchi



View Online



Export Citation



CrossMark

ARTICLES YOU MAY BE INTERESTED IN

Multiferroics: Past, present, and future

Physics Today **63**, 38 (2010); <https://doi.org/10.1063/1.3502547>

Multiferroic magnetoelectric composites: Historical perspective, status, and future directions

Journal of Applied Physics **103**, 031101 (2008); <https://doi.org/10.1063/1.2836410>

Magnetic microscopy and simulation of strain-mediated control of magnetization in PMN-PT/Ni nanostructures

Applied Physics Letters **109**, 162404 (2016); <https://doi.org/10.1063/1.4965028>

additive manufacturing epitaxial crystal growth cerium oxide polishing powder silver nanoparticles sputtering targets

III-V semiconductors CVD precursors europium phosphors

InAs wafers laser crystals ultra high purity materials MOFs

rare earth metals photovoltaics refractory metals MOCVD

superconductors transparent ceramics ultra high purity silicon

American Elements opens up a world of possibilities so you can **Now Invent!**

Over 15,000 certified high purity laboratory chemicals, metals, & advanced materials and a state-of-the-art Research Center. Printable GHS-compliant Safety Data Sheets. Thousands of new products. And much more. All on a secure multi-language "Mobile Responsive" platform.

gallium lump glassy carbon nanodispersions

surface functionalized nanoparticles

organometallics quantum dots

perovskite crystals yttrium iron garnet alternative energy h-BN

gold nanocubes graphene oxide macromolecules photonics

rhodium sponge fiber optics beamsplitters infrared dyes zeolites

fused quartz metallocenes platinum ink buckyballs Ti-6Al-4V

AMERICAN ELEMENTS
THE ADVANCED MATERIALS MANUFACTURER®

deposition slugs OLED lighting spintronics solar energy

osmium nanoribbons thin films chalcogenides AuNPs

GDC Li-ion battery electrolytes 99.999% ruthenium spheres

endothelial fullerenes copper nanoparticles diamond micropowder

CIGS MBE grade materials palladium catalysts flexible electronics

beta-barium borate borosilicate glass dysprosium pellets YBCO

pyrolytic graphite 3d graphene foam indium tin oxide mesoporous silica

raman substrates sapphire windows tungsten carbide InGaAs

barium fluoride carbon nanotubes lithium niobate scandium powder

Now Invent.™
The Next Generation of Material Science Catalogs

www.americanelements.com



Simultaneous imaging of the ferromagnetic and ferroelectric structure in multiferroic heterostructures

J. Unguris,^{1,a} S. R. Bowden,^{1,2} D. T. Pierce,¹ M. Trassin,^{3,4} R. Ramesh,^{3,5} S.-W. Cheong,⁶ S. Fackler,⁷ and I. Takeuchi⁷

¹Center for Nanoscale Science and Technology, National Institute of Standards and Technology, Gaithersburg, Maryland 20899, USA

²Maryland Nanocenter, University of Maryland, College Park, Maryland 20742, USA

³Department of Materials Science and Engineering, University of California, Berkeley, California 94720, USA

⁴Department of Materials, Swiss Federal Institute of Technology Zürich, 8093 Zürich, Switzerland

⁵Department of Physics, University of California, Berkeley, California 94720, USA

⁶Rutgers Center for Emergent Materials and Department of Physics and Astronomy, Rutgers University, Piscataway, New Jersey 08854, USA

⁷Department of Materials Science and Engineering, University of Maryland, College Park, Maryland 20742, USA

(Received 12 June 2014; accepted 2 July 2014; published online 18 July 2014)

By measuring the spin polarization of secondary electrons and the intensity of backscattered electrons generated in a scanning electron microscope, we are able to simultaneously image the ferromagnetic domain structure of a ferromagnetic thin film and the ferroelectric domain structure of the underlying ferroelectric substrate upon which it is grown. Simultaneous imaging allows straightforward, quantitative measurements of the correlations in these complex multiferroic systems. We have successfully imaged domains in CoFe/BFO and Fe/BTO, two systems with very different ferromagnet/ferroelectric coupling mechanisms, demonstrating how this technique provides a new local probe of magneto electric/strictive effects in multiferroic heterostructures. © 2014 Author(s). All article content, except where otherwise noted, is licensed under a Creative Commons Attribution 3.0 Unported License. [<http://dx.doi.org/10.1063/1.4890055>]

Combining ferromagnetic and ferroelectric materials has produced exciting new opportunities to design and produce structures with new functionalities.¹⁻³ In particular, heteroepitaxially grown ferromagnetic/ferroelectric multilayers provide a potential path towards making nanodevices where the magnetization is electrically controlled through magnetoelastic or magnetoelectric coupling.⁴⁻⁶ In these multilayer heterostructures knowledge about the magnetization and polarization at the interface is key to understanding how these coupling mechanisms work. For example, one needs to see how the domain structure of a ferromagnetic thin film is correlated with and influenced by the domain structure of an underlying ferroelectric substrate. Various experimental techniques are currently used to image the ferroelectric and ferromagnetic structures: piezo-response force microscopy (PFM),⁷ x-ray linear dichroism photoemission electron microscopy (XLD-PEEM),⁸ Low-Energy Electron Microscopy (LEEM),⁹ and optical birefringence¹⁰ have been used to reveal the ferroelectric domain structures, while techniques such as magnetic force microscopy (MFM), magneto-optical Kerr microscopy (MOKE), and x-ray magnetic circular dichroism photoemission electron microscopy (XMCD-PEEM) have all been used to image ferromagnetic domain structure.¹¹ A detailed, quantitative analysis of ferromagnetic/ferroelectric domain structural correlations, however, is sometimes

^aAuthor to whom correspondence should be addressed. Electronic mail: john.unguris@nist.gov

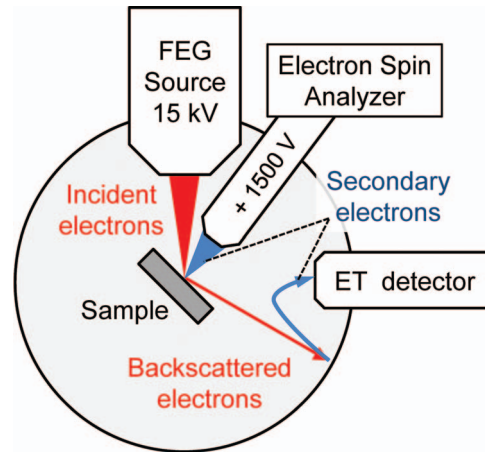


FIG. 1. Schematic of the SEM showing the field emission (FE) source of the incident electron beam, the SEMPA analyzer used to spin-analyze the secondary electrons from the sample, and the Everhart-Thornley (ET) detector used to indirectly measure the BSE intensity by measuring secondaries generated away from the sample.

difficult since the images are usually not acquired simultaneously, or even under similar conditions. For example, PFM imaging can only be used when the conductive ferromagnetic film is not present.

In this paper, we demonstrate the simultaneous imaging of ferromagnetic and ferroelectric structure in multiferroic multilayers using a modified scanning electron microscope (SEM). The low energy secondary electrons are spin-polarized and provide information about the direction of the magnetization in the ferromagnetic film, while the high energy elastically scattered electrons are sensitive to crystal structure and lattice distortions and hence the electric polarization direction in the underlying ferroelectric substrate. We have successfully applied this technique to $\text{Co}_{0.9}\text{Fe}_{0.1}$, $\text{Ni}_{0.8}\text{Fe}_{0.2}$, and Fe thin films, from 2 to 100 nm thick, deposited on multiferroic BiFeO_3 (BFO) films and ferroelectric BaTiO_3 (BTO) substrates. The observed correlations between ferromagnetic and ferroelectric structures varied greatly; they were very pronounced for thin CoFe films on BFO films and weak for thick NiFe films on bulk BTO crystals.

The schematic in Fig. 1 shows how the different energy scattered electrons are collected. The incident 15 keV electron beam generates low energy secondary electrons and high energy, elastically scattered electrons usually referred to as backscattered electrons (BSE). The secondary electrons generated at the sample are spin polarized and the polarization is directly proportional to the magnetization. This is the basis of the magnetic imaging technique, scanning electron microscopy with polarization analysis (SEMPA).¹² The front end of the SEMPA spin analyzer optics is biased at +1500 V and thereby collects all of the secondary electrons generated at the sample. The escape depth of these secondary electrons is about 1 nm so that SEMPA probes the outermost few atomic layers of the sample. On the other hand, elastically scattered BSE probe much deeper into the sample, on the order of 100 nm at these energies.¹³ For well-ordered, crystalline samples, the BSE intensities are sensitive to the scattering geometry, since electron diffraction and electron channeling play important roles in the elastic scattering process. This sensitivity to crystal structure is the basis for the ferroelectric structure contrast. Ferroelectric domains polarized in different directions also have crystal structures that are distorted in different directions and therefore different channeling and diffraction conditions. This BSE sensitivity to scattering geometry has been used in previous experiments to image ferroelectric domain structures in uncoated samples using a standard BSE detector in an SEM.¹⁴ In our measurements, the BSE intensity is measured using a second secondary electron detector in the following manner: Most of the BSE emitted from the sample are not collected by the SEMPA analyzer. Instead, these BSE strike surfaces inside the vacuum chamber, such as the chamber walls, and convert to secondary electrons which are then collected by the SEM's standard Everhart-Thornley (ET) secondary electron detector.

An example of a measurement is shown in Fig. 2. In this case, the sample is a patterned 2 nm thick $\text{Co}_{0.9}\text{Fe}_{0.1}$ film disc deposited on a 100 nm thick BFO (001)-oriented film epitaxially

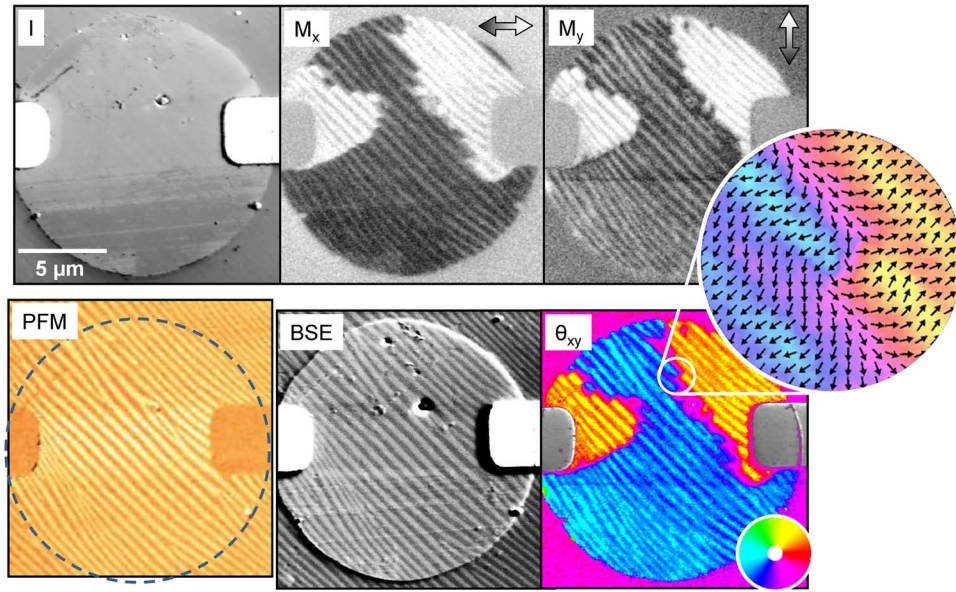


FIG. 2. SEMPA, BSE, and PFM images of a 15 μm diam. CoFe disc on a BFO substrate. The SEMPA measured secondary electron intensity, in-plane components of the magnetization, and the derived magnetization direction are shown in I, M_x , M_y , and θ_{xy} . The magnetization direction is given by the colors in the color wheel shown in the θ_{xy} image and by the arrows in the magnified inset. Simultaneously measured BSE intensity is shown in BSE. PFM shows a PFM image of the disc after removing the CoFe film.

grown by pulsed laser deposition (PLD) on a 8 nm thick SrRuO₃ (SRO) buffered DyScO₃ (DSO) (110)-oriented substrate (see the supplementary material).¹⁵ This strained heterostructure produces a simplified ferroelectric domain pattern consisting of 71° stripe domains in the BFO with two orthogonal in-plane projections of the electric polarization.¹⁶ By analyzing the spin polarization of the secondary electrons from the sample, SEMPA simultaneously measures the intensity, I, and the two in-plane magnetization components, M_x and M_y , of the CoFe film. From these components, the in-plane magnetization direction, $\theta_{xy} = \tan^{-1}(M_x/M_y)$, is determined with a one standard deviation uncertainty of $\pm 3^\circ$. (No significant out-of-plane polarization, M_z , was observed.)

A simultaneously acquired image using the backscattered electron intensity, BSE, is also shown in Fig. 2. The BSE image contrast reveals the BFO ferroelectric domain structure both in the region covered by the CoFe disc and for the uncovered BFO. Unlike the SEMPA or PFM image, however, the BSE image does not give the absolute direction of the polarization. The BSE contrast is only sensitive to lattice distortions. To see how well the BSE image shows the ferroelectric structure, the CoFe films were removed by ion milling and the ferroelectric domain structure of the uncoated samples was imaged using PFM. Although the BSE image is sensitive to a few other topographic and compositional features, comparison of the BSE and PFM images in Fig. 2 clearly shows that the BSE image reveals the same ferroelectric structure as the PFM image.

Simultaneous measurements of the ferromagnetic and ferroelectric structures provide quantitative information about the correlations and coupling between the two systems. For example, Fig. 3 shows SEMPA and BSE images of an unpatterned CoFe film grown on a BFO sample similar to the one shown in Fig. 2. The film is in the as-grown state (before applying a magnetic field), so that the ferromagnetic structure is somewhat more complex than in Fig. 2, but the influence of the striped ferroelectric domains of the underlying BFO is unmistakable. A more quantitative comparison is provided by the line scans shown in Fig. 3. These line scans from exactly the same areas of the sample show that the degree to which the magnetic structure follows the ferroelectric structure depends on the size of the underlying BFO stripe domains. Without intralayer exchange coupling, the CoFe magnetization direction should follow the BFO domains exactly, alternating between $+45^\circ$ to -45° in the adjacent stripes. The CoFe magnetization comes close to this behavior when the BFO stripes

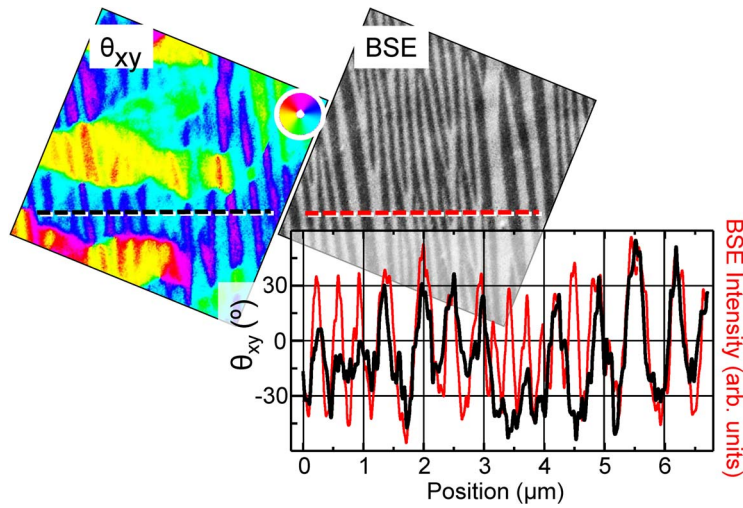


FIG. 3. Comparison of ferromagnetic (θ_{xy}) and ferroelectric (BSE) structure from CoFe/BFO. Line scans show the magnitude of the magnetic fluctuations and the correlation between magnetic and ferroelectric oscillations.

are wider than about 400 nm. However, the angles are reduced in narrower stripes, and for stripes less than about 100 nm wide, the CoFe magnetization does not follow the BFO stripe structure at all. These measurements show that the intralayer exchange coupling, even in CoFe films that are only 2 nm thick, plays an important role in determining how the ferromagnetic film responds to the ferroelectric. The resulting magnetic structure is therefore a balance between exchange which tends to keep the magnetization uniform and magnetoelectric coupling which follows the ferroelectric polarization. For this system, the SEMPA/BSE measurements along with micromagnetic modeling were used to determine the effective coupling strength of 7 (+2.5, -1.5) mT between the ferromagnet and the ferroelectric.¹⁷

To test the sensitivity of the BSE imaging contrast to switching of the ferroelectric polarization state, patterned samples were imaged after applying voltages that were sufficient to reverse the polarization. Figure 4 shows an example of such a measurement on a structure similar to the one shown in Fig. 2 except with a 200 nm thick BFO layer. In this case, the SEMPA, BSE, and PFM images were acquired after first applying a 7 V (350 kV/cm) pulse using the patterned CoFe film as the top electrode and the SRO as the bottom electrode. After the SEMPA and BSE images were acquired, the CoFe was removed by ion milling and the sample was imaged by PFM. The PFM image clearly shows that the polarization under the disc has been reversed, but the BSE image is less clear. Relative to the BSE polarization contrast outside the disc, the contrast under the disc has decreased rather than reversed. This is not surprising, since the sample was oriented to optimize the BSE contrast for the unswitched lattice structure, and the diffraction and back-scattering conditions for the lattice structure after switching may not produce optimal BSE contrast. This is a consideration when using this technique to image multiferroic states while switching devices with electric or magnetic fields. The SEMPA images will clearly show whether the ferromagnetic state has changed, but the BSE image may not unambiguously reveal reversals of the ferroelectric polarization where the switched polarization is along the same axis.

The measurement examples that have been presented in this paper so far have all been from the same multilayer structure: a thin, several nm thick, CoFe film on a strained, stripe domain, BFO substrate. The SEMPA/BSE technique has also been successfully applied to other ferromagnet/ferroelectric systems, and three of those are shown in Fig. 5: (i) 2 nm of $\text{Co}_{0.9}\text{Fe}_{0.1}$ on strain relieved 4-variant BFO, (ii) 3 nm of Fe on a (001) BaTiO_3 (BTO) single crystal, and (iii) 100 nm of $\text{Ni}_{0.8}\text{Fe}_{0.2}$ on a BTO crystal. Each of these examples illustrates different features of the SEMPA/BSE measurement technique. Specifically:

- (i) By growing BFO on a thicker, thus relaxed, 20 nm thick SRO buffer the strain responsible for the striped, two-variant structure is relieved and the BFO forms the more complex four-variant

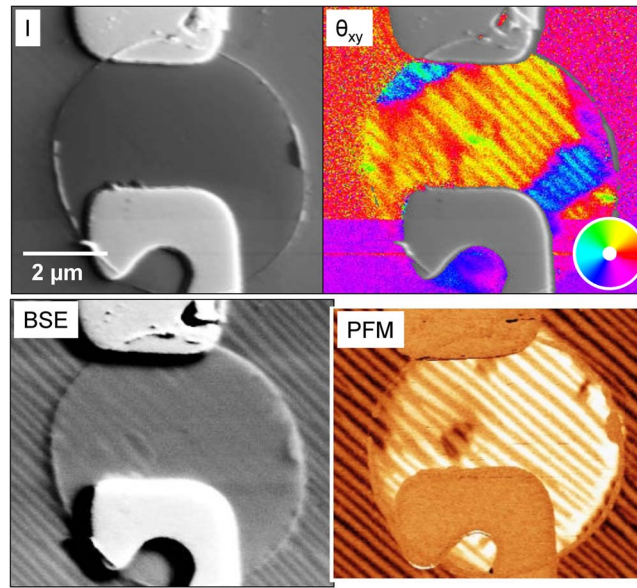


FIG. 4. SEMPA (I and θ_{xy}), BSE, and PFM images of a 6 μm diam. CoFe/BFO disc after applying a 7 V pulse to reverse the polarization. The PFM image was acquired after removing the CoFe.

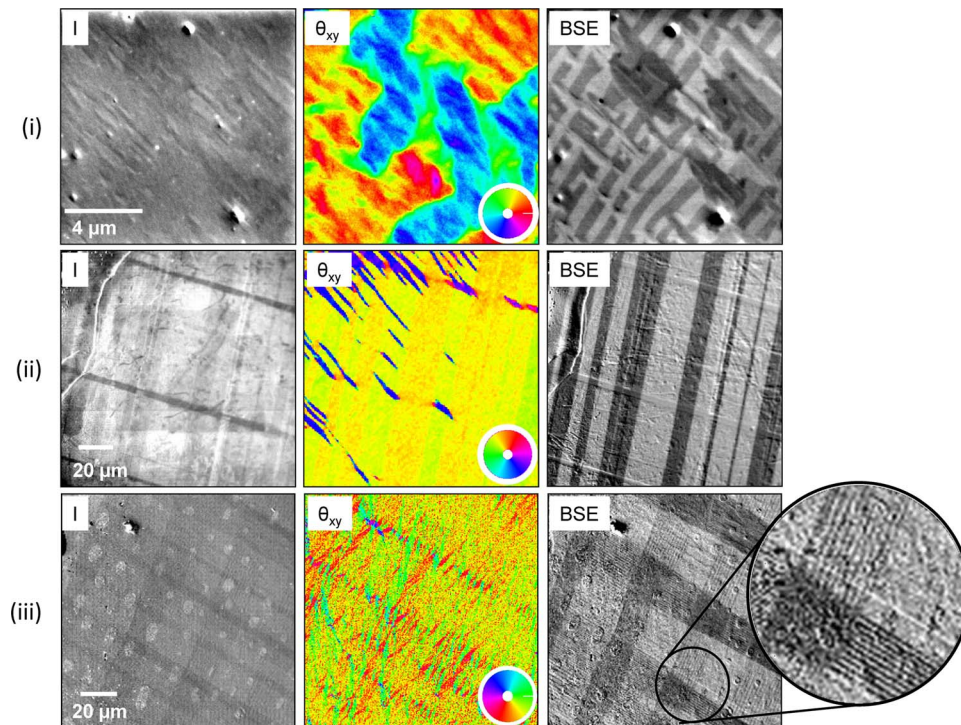


FIG. 5. SEMPA (I and θ_{xy}) and BSE images from three different samples: (i) 2 nm $\text{Co}_{0.9}\text{Fe}_{0.1}$ on strain relieved 4-variant BFO, (ii) 3 nm Fe on (001) BTO, and (iii) 100 nm of $\text{Ni}_{0.8}\text{Fe}_{0.2}$ on BTO. Inset shows an enlargement of the lamellar structure.

ferroelectric domain structure seen in the BSE image in Fig. 5(i). The ferroelectric structures of these films have been analyzed previously using XLD-PEEM¹⁸ and PFM.¹⁹ In these measurements, the direction of the polarization was determined by imaging the ferroelectric domain structure at various angles with a technique of known directional sensitivity. This is not possible in the current SEMPA/BSE imaging arrangement. So, while the ferroelectric domains are

clearly visible in the BSE image, we cannot determine the absolute polarization directions. On the other hand, the simultaneously acquired SEMPA image clearly shows the magnetization direction. Surprisingly, the magnetization does not follow the four variant ferroelectric pattern, but instead looks more like the striped magnetic structure on the two variant strained BFO.

- (ii) Unlike BFO where magnetoelectric coupling dominates, BTO is not a multiferroic and any coupling to a ferromagnetic film is expected to be through strain mediated magnetostriction. In this example, a 3 nm thick Fe film was deposited *in situ* on a BTO (001) substrate after the BTO was first etched using aqua regia and then cleaned *in situ* using 50 eV Ar ions. Twin boundaries along (101) and (011) planes in the tetragonally distorted BTO are responsible for domain walls where the polarization changes direction by 90° .¹⁰ These ferroelectric domains are clearly visible in the BSE image in Fig. 5. Using information about this sample's crystallographic orientation, we can identify the domains as alternating stripes of so-called **a** and **c** domains with polarizations in-plane and perpendicular to the surface, respectively. One cannot determine which stripe is an **a** domain or a **c** domain from the BSE image, however. Furthermore, it is also not clear if the BSE image is sensitive to 180° reversals of the polarization direction. In this case, the BSE contrast would have to originate from the small displacement of the Ti atom rather than the larger tetragonal distortion of the Ba lattice. The SEMPA image shows that the ferroelectric structure is imprinted on the Fe film magnetization, albeit relatively weakly. In MOKE studies²⁰ of similar structures, $\text{Co}_{0.6}\text{Fe}_{0.4}(15\text{ nm})/\text{BTO}$, it was concluded that the strain transfer at the interface was less than 10% in contrast to most reports on strain-mediated coupling where 100% transfer is assumed. These MOKE results together with the weak imprint seen in Fig. 5(ii), and our observation that the degree of imprinting depended sensitively on BTO substrate preparation and annealing, suggest that, even in this strain-mediated system, the atomic scale order of the Fe/BTO interface is critical. An interface-controlled, thickness dependent investigation of the strain-mediated coupling using the SEMPA/BSE approach is warranted.
- (iii) In this sample, a relatively thick, 100 nm $\text{Ni}_{0.8}\text{Fe}_{0.2}$ film was grown on a BTO (001) substrate. The domain structure of the ferroelectric is still visible in the BSE image, even through this thick, polycrystalline ferromagnetic coating. In this case, the structure reveals bands of laminar groups of twin boundaries that intersect at right angles.²¹ The SEMPA magnetization image reveals some subtle influences from the underlying ferroelectric structure, but the magnetization also shows characteristics, such as magnetization ripple, of an uncoupled ferromagnetic film. This is reasonable, since we expect strain mediated coupling effects to be significantly relaxed and bulk magnetic properties to override the interfacial coupling for thicker ferromagnetic films.

We have looked at a number of different multiferroic heterostructures which illustrate the major strengths, and some limitations, of imaging ferromagnetic/ferroelectric domains using the combined SEMPA/BSE techniques. As mentioned above, a limitation of the BSE image is that it does not give the direction of polarization, and the SEMPA image derives from the magnetization of the top few layers requiring a clean surface. Additionally, although electric fields can be applied during a SEMPA measurement, magnetic fields cannot. The major strength of the SEMPA/BSE technique is that the information regarding the magnetic and ferroelectric domains is acquired simultaneously but separately. Our results from various ferromagnet/ferroelectric heterostructure combinations demonstrate that it is possible to obtain high resolution images of magnetic microstructure and simultaneously look through ferromagnetic films over a wide range of thicknesses (up to 100 nm in Fig. 5(iii)) and image the underlying ferroelectric domain structure. We expect that future studies comparing SEMPA and BSE images will provide important information on coupling, whether it is exchange coupling, strain-mediated coupling, or both. In addition, for patterned heterostructures with electrical contacts it should also be possible to image electrically controlled ferroelectric/ferromagnetic devices *in situ*.

In conclusion, we have shown that measuring the BSE intensity and the secondary electron polarization in a SEM allows us to simultaneously image the magnetic and ferroelectric structure in multilayer multiferroics. As multiferroic materials and thin films make strides towards eventual

device applications, a robust and versatile diagnostic tool will be needed. The SEMPA/BSE images directly and quantitatively measure magnetization/polarization correlations, and thereby provide a new probe of magnetoelectric/magnetostrictive coupling and switching mechanisms in new materials and devices consisting of multilayer multiferroic heterostructures.

We thank M. D. Stiles for discussions. S. R. Bowden acknowledges support from the National Research Council and from the Cooperative Research Agreement between the University of Maryland and the National Institute of Standards and Technology Center for Nanoscale Science and Technology (Award No. 70NANB10H193 through the University of Maryland). M. Trassin acknowledges support from the Center for Energy Efficient Electronics Science (NSF Grant No. 0939514). S. Fackler acknowledges support of the Maryland NanoCenter and its NanoLab. The work at Rutgers was supported by the NSF under Grant No. NSF-DMR-1104484.

- ¹N. A. Spaldin, S-W. Cheong, and R. Ramesh, *Phys. Today* **63**, 38 (2010).
- ²M. Bibes and A. Barthélemy, *Nat. Mater.* **7**, 425 (2008).
- ³W. Erenstein, N. D. Mathur, and J. F. Scott, *Nature (London)* **442**, 759 (2006).
- ⁴R. Ramesh and N. A. Spaldin, *Nat. Mater.* **6**, 21 (2007).
- ⁵T. H. E. Lahtinen, K. J. A. Franke, and S. van Dijken, *Sci. Rep.* **2**, 258 (2012).
- ⁶J. T. Heron, M. Trassin, K. Ashraf, M. Gajek, Q. He, S. Y. wang, D. E. Nikonov, Y-H. Chu, S. Salalhudin, and R. Ramesh, *Phys. Rev. Lett.* **107**, 217202 (2011).
- ⁷S. V. Kalinin and D. A. Bonnell, *Phys. Rev. B* **65**, 125408 (2002).
- ⁸T. Zhao, A. Scholl, F. Zavaliche, K. Lee, M. Barry, A. Doran, M. P. Cruz, Y. H. Chu, C. Ederer, N. A. Spaldin, R. R. Das, D. M. Kim, S. H. Baek, C. B. Eom, and R. Ramesh, *Nat. Mater.* **5**, 823 (2006).
- ⁹N. Barrett, J. E. Rault, J. L. Wang, C. Mathieu, A. Locatelli, T. O. Montes, M. A. Nino, S. Fusil, M. Bibes, A. Barthelemy, D. Sand, W. Ren, S. Prosandeev, L. Bellaiche, B. Vilquin, A. Petaru, I. P. Krug, and C. M. Schneider, *J. Appl. Phys.* **113**, 187217 (2013).
- ¹⁰R. D. Dragsdorf and J. C. Crawford, *J. Appl. Phys.* **36**, 1934 (1965).
- ¹¹For a review of magnetic imaging techniques, see *Magnetic Microscopy of Nanostructures*, edited by H. Hopster and H. P. Oepen (Springer-Verlag, Berlin, 2005).
- ¹²M. R. Scheinfein, J. Unguris, M. H. Kelley, D. T. Pierce, and R. J. Celotta, *Rev. Sci. Instrum.* **61**, 2501 (1990).
- ¹³L. Reimer, *Scanning Electron Microscopy Physics of Image Formation and Microanalysis* (Springer-Verlag, Berlin, 1998).
- ¹⁴D. Grüner and Z. Shen, *J. Am. Ceram. Soc.* **93**, 48 (2010).
- ¹⁵See supplementary material at <http://dx.doi.org/10.1063/1.4890055> for sample preparation and imaging details.
- ¹⁶Y. H. Chu, Q. He, C. H. Yang, P. Yu, L. W. Martin, P. Shafer, and R. Ramesh, *Nano Lett.* **9**, 1726 (2009).
- ¹⁷M. Trassin, J. D. Clarkson, S. R. Bowden, Jian Liu, J. T. Heron, R. J. Paull, E. Arenholz, D. T. Pierce, and J. Unguris, *Phys. Rev. B* **87**, 134426 (2013).
- ¹⁸M. B. Holcomb, L. W. Martin, A. Scholl, Q. He, P. Yu, C.-H. Yang, S. Y. Yang, P.-A. Glans, M. Valvidares, M. Huijben, J. B. Kortright, J. Guo, Y.-H. Chu, and R. Ramesh, *Phys. Rev. B* **81**, 134406 (2010).
- ¹⁹F. Zavaliche, S. Y. Yang, T. Zhao, Y. H. Chu, M. P. Cruz, C. B. Eom, and R. Ramesh, *Phase Transitions* **79**, 991 (2006).
- ²⁰T. H. E. Lahtinen, J. O. tuomi, and S. van Dijken, *IEEE Trans. Magn.* **47**, 3768 (2011).
- ²¹W. Forsbergh, *Phys. Rev.* **76**, 1187 (1949).